IOP Publishing Modelling and Simulation in Materials Science and Engineering
Modelling Simul. Mater. Sci. Eng. **26** (2018) 065012 (15pp) https://doi.org/10.1088/1361-651X/aad20b

Computational modeling of crystallographic texture evolution over cubochoric space

Pınar Acar[1], **Veera Sundararaghavan**[2] and **Marc De Graef**[3]

[1] Mechanical Engineering, Virginia Tech, Blacksburg, VA 24061, United States of America
[2] Aerospace Engineering, University of Michigan, Ann Arbor, MI 48109, United States of America
[3] Materials Science and Engineering, Carnegie Mellon University, Pittsburgh, PA 15213, United States of America

E-mail: pacar@vt.edu

Received 15 January 2018, revised 21 June 2018
Accepted for publication 9 July 2018
Published 1 August 2018

Abstract

The present work addresses representation of texture evolution in face-centered cubic (fcc) microstructures in cubochoric orientation space. The microstructure is quantified with the orientation distribution function (ODF), which models volume density in the fundamental region of crystallographic space. The ODF is discretized using a finite element scheme in the cubochoric fundamental region. This scheme shows superior features over the classical techniques in global spaces, such as spherical harmonics or Fourier space solutions, since it can represent a large variety of textures, including very sharp textures such as a single crystal. The texture evolution during a particular deformation process is associated with the evolution of the ODF in time, which is governed by the conservation equation and crystal constitutive relations. The transformation in between cubochoric space and other popular angle-axis representation such as Rodrigues space is performed with a two-step approach including the transformations from Rodrigues domain to homochoric domain, and homochoric domain to cubochoric domain through a numerical scheme. The ODF evolution in an fcc material during different deformation processes, such as tension, plane strain compression and shear, is compared across both Rodrigues and cubochoric spaces, and similar patterns are observed.

Keywords: texture evolution, cubochoric space, microstructure

(Some figures may appear in colour only in the online journal)

1. Introduction

The prediction of texture evolution in a deformation process has attracted significant interest in the scientific literature since, during this process, the material properties also evolve in a way that strongly depends on the underlying microstructure. There have been several computational and experimental studies particularly focusing on texture evolution in face-centered cubic (fcc) materials. Some of the efforts concentrate on modeling the texture evolution with discrete aggregate models [1–5]. Other studies model the texture evolution by quantifying the microstructure with probabilistic descriptors [6, 7]. The microstructure modeling of the present work is also based on the quantification of the microstructure using a probabilistic descriptor, namely the orientation distribution function (ODF). The ODF represents the volume densities of crystals of different orientations in the microstructure. The ODF is defined based on a parameterization of the crystal lattice rotation. Popular representations include Euler angles [8, 9] and classes of angle-axis representations, with the most popular being the Rodrigues parameterization [10]. Conversion of continuous orientation space to finite degrees of freedom for material property optimization requires discretization techniques. Discretization schemes either focus on a global basis (e.g., Fourier space or spherical harmonics [11, 12]) or a local basis using a finite element discretized Rodrigues space with polynomial shape functions defined locally over each element [13, 14]. In [15], the discrete harmonics and finite elements over the Rodrigues orientation space have been exercised for multi-scale embedding of polycrystal plasticity. The finite element discretization of the ODF can be found in detail in earlier works of the authors [6, 16]. The main goal of the present work is to represent the ODF evolution in cubochoric space. Cubochoric space is the preferred orientation representation for dictionary based indexing of crystalline diffraction patterns since this indexing approach requires a uniform sampling of orientation space [17, 18]. The previously available algorithms for uniform sampling, such as the Hopf fibration (Yershova and LaValle [19], Yershova *et al* [20]) and the hierarchical equal area iso-latitude pixelization (HEALPix) framework (Gorski *et al* [21]) are not suitable in terms of accounting for crystallographic symmetries. Therefore a new indexing strategy was adapted by Chen *et al* [17] beginning with a simple 3D cubic grid which is mapped uniformly onto SO(3) (Roşca *et al* [22]). The proposed framework can be applied to any diffraction technique which allows for the extraction of the orientation of the diffracting volume, such as electron backscatter diffraction, precession electron diffraction or electron channeling patterns [18]. Singh and De Graef [18] populated a diffraction dictionary with patterns uniformly covering the range of possible patterns. They represented the 3D rotations in cubochoric space so as to generate uniform samples of 3D rotations with a straightforward gridding procedure. Numerically, the transformation between Rodrigues space and cubochoric space requires an intermediate transformation to homochoric space; computational details on the transformation from the homochoric domain to cubochoric coordinates can be found in [18].

The primary goal of the present work is to represent the texture evolution in cubochoric space with comparison with Rodrigues representation. Some of the important deformation processes, such as the texture evolution during tension, plane strain compression and shear tests, were analyzed for this purpose. First, the finite element representation which was used to discretize the ODFs in the Rodrigues domain, which was then transformed into cubochoric space. The transformation was also applied to the constitutive relations to compute the reorientation velocity in cubochoric coordinates. The texture evolution in each of the aforementioned deformation processes was represented in both Rodrigues and cubochoric spaces, and the ODF evolutions were found to be comparable. The organization of the paper is as follows: section 2 discusses the basics of texture evolution over Rodrigues space and

crystal constitutive equations. In section 3, the numerical procedure for the transformation from the Rodrigues domain to cubochoric space is provided. Section 3 also discusses the adaptation of the crystal constitutive equation to cubochoric space. Example applications of the texture evolution in both Rodrigues and cubochoric spaces are included in section 4. Section 5 concludes the study with a summary and possible future extensions.

2. Texture evolution over Rodrigues space

The complete orientation space of a polycrystal can be reduced to a smaller subset, called the fundamental region or fundamental zone, as a consequence of crystal symmetries. With in the fundamental region, each crystal orientation is represented uniquely by a coordinate $\boldsymbol{r}$, the parameterization for the rotation (e.g., Euler angles, Rodrigues vector etc). The ODF, represented by $\mathcal{A}(\boldsymbol{r})$, describes the volume density of crystals of orientation $\boldsymbol{r}$ in a discrete space. The volume density of any other node outside the fundamental region can be obtained from these independent nodes through symmetry operations.

2.1. Rodrigues fundamental region

The turning of an object or a coordinate system by a given angle ϕ about a fixed point, $\boldsymbol{d}$, is described as a rotation. Each rotation is represented by the unit vector $\boldsymbol{n}$, which is known as the rotation axis. In this work we assume that a rotation is fully defined by $\boldsymbol{d}$, $\boldsymbol{n}$ and ϕ. The rotation angle, ϕ, is considered to be positive for a counter-clockwise rotation, and the fixed point, $\boldsymbol{d}$, is assumed to coincide with the origin of the reference frame such that $\boldsymbol{d} = \boldsymbol{0}$.

The use of Rodrigues representation is favorable compared to the widely used Euler angles since the Euler angles can introduce singularities. The Rodrigues domain implements an angle-axis representation based on the unique representation of an orientation with rotation axis $\boldsymbol{n}$, and a rotation angle ϕ about the axis. The Rodrigues parameters can be identified by scaling the axis of rotation as follows:

$$\boldsymbol{r} = \boldsymbol{n}f = \boldsymbol{n}\tan\frac{\phi}{2}, \tag{1}$$

where f is the angle dependent function.

For modeling crystal orientation, positive rotation angles are represented by points along the line indicated with the unit vector, $\boldsymbol{n}$; however, negative rotation angles are converted to the negative of the unit vector, $\boldsymbol{n}$, and a positive rotation angle. The restriction of the rotation angle to a positive values is advantageous since in this case $\tan(\phi/2)$ is always positive, and equal to the length of the Rodrigues vector.

The relation between the Rodrigues orientation parameters, $\boldsymbol{r}$, and the rotation matrix, $\boldsymbol{R}$, is represented in equation (2):

$$\boldsymbol{R} = \frac{1}{1 + \boldsymbol{r}\cdot\boldsymbol{r}}(\boldsymbol{I}(1 - \boldsymbol{r}\cdot\boldsymbol{r}) + 2(\boldsymbol{r}\otimes\boldsymbol{r} + \boldsymbol{I}\times\boldsymbol{r}); \tag{2}$$

the symbol $\boldsymbol{I}$ represents the identity matrix. The reorientation velocity, $\boldsymbol{v}$, expression can be obtained using the incremental change in the orientation, $\boldsymbol{r}$, due to crystal lattice spin and is described by:

$$\boldsymbol{v} = \frac{1}{2}(\boldsymbol{\omega} + (\boldsymbol{\omega}\ \cdot\ \boldsymbol{r})\boldsymbol{r} + \boldsymbol{\omega}\times\boldsymbol{r}), \tag{3}$$

where $\boldsymbol{\omega}$ represents the spin vector defined as $\boldsymbol{\omega} = \text{vect}(\dot{\boldsymbol{R}}^e \boldsymbol{R}^{eT}) = \text{vect}(\boldsymbol{\Omega})$ where $\boldsymbol{\Omega}$ is the spin tensor, and $\boldsymbol{R}^e$ is evaluated through the polar decomposition of the elastic deformation gradient, $\boldsymbol{F}^e$, as $\boldsymbol{F}^e = \boldsymbol{R}^e \boldsymbol{U}^e$.

The discretization of the ODF is based on the use of Rodrigues parameters in the finite element mesh. The fundamental region is discretized into N independent nodes with N_{elem} finite elements (and N_{int} integration points per element). The ODF is normalized to unity over the fundamental region as [16]:

$$\int_{\mathcal{R}} \mathcal{A}\, \mathrm{d}\boldsymbol{v} = \sum_{n=1}^{N_{\text{elem}}} \sum_{m=1}^{N_{\text{int}}} A(\boldsymbol{r}_m) w_m |J_n| \frac{1}{(1 + \boldsymbol{r}_m \cdot \boldsymbol{r}_m)^2} = 1, \tag{4}$$

where $A(\boldsymbol{r}_m)$ is the value of the ODF at the mth integration point with global coordinate $\boldsymbol{r}_m$, $|J_n|$ is the Jacobian determinant of the nth element and w_m is the integration weight associated with the mth integration point. The final factor represents the metric of the Rodrigues parameterization.

2.2. Modeling texture evolution

The texture evolution over the Rodrigues fundamental region is driven by the evolution of the ODF, which, in turn, is governed by the ODF conservation equation. In this work, we utilize the Lagrangian form of the ODF evolution equation. When deformed, the ODF changes due to reorienting of grains. The probabilities are evolved from time $t = 0$ corresponding an initial ODF. The initial orientation $\boldsymbol{r}_o$ of a crystal reorients during deformation and maps to a new orientation $\boldsymbol{r}_t$ at time t. It is assumed that the mapping from $\boldsymbol{r}_o$ to $\boldsymbol{r}_t$ is invertible. The ODF, $A(\boldsymbol{r}_t)$, represents the volume density of crystals with orientation $\boldsymbol{r}_t$ at time t. The evolution of the ODF is given by the conservation equation (5) as:

$$\int A(\boldsymbol{r}_o, t = 0) \mathrm{d}\boldsymbol{r}_o = \int A(\boldsymbol{r}_t) \mathrm{d}\boldsymbol{r}_t = 1, \tag{5}$$

where $\mathrm{d}\boldsymbol{r}_o$ represents the volume element in the undeformed (initial) ODF mesh, which becomes volume element $\mathrm{d}\boldsymbol{r}_t$ at time t. A Jacobian $J(\boldsymbol{r}_o, t) = \det(\boldsymbol{G})$ gives the ratio of elemental volumes, where $\boldsymbol{G}$ is the reorientation gradient given as $\boldsymbol{G}(\boldsymbol{r}_o, t) = \frac{\partial \boldsymbol{r}_t}{\partial \boldsymbol{r}_o}$. Using the Jacobian, a map of the current mesh (at time t) to the reference mesh (at $t = 0$) can be made:

$$\int (A(\boldsymbol{r}_o, t = 0) - \hat{A}(\boldsymbol{r}_o, t) J(\boldsymbol{r}_o, t)) \mathrm{d}\boldsymbol{r}_o = 0. \tag{6}$$

The quantity written as $\hat{A}(\boldsymbol{r}_o, t)$ is the volume density $A(\boldsymbol{r}_t)$ plotted over the corresponding orientation ($\boldsymbol{r}_o$) in the initial mesh. Thus, $\hat{A}(\boldsymbol{r}_o, t)$ gives the Lagrangian representation of the current ODF in the initial mesh. If the integrand is continuous, a localized relationship of the following form can be used to update the ODF at any time t:

$$\hat{A}(\boldsymbol{r}_o, t) J(\boldsymbol{r}_o, t) = A(\boldsymbol{r}_o, t = 0). \tag{7}$$

For computing $\boldsymbol{r}_t$, a reorientation velocity is obtained. The reorientation velocity can be calculated using the constitutive model. However, it should be calculated using the cubochoric coordinates to perform the finite element simulation in the cubochoric space. In the Lagrangian ODF evolution formulation, the Jacobian can be interpreted as the ratio of elemental 3D volumes. If the element volume decreases over time, the probability density has to increase based on equation (4) to maintain normalization of the ODF. The integrand in equation (6) needs to be continuous for the localization relationship to be valid. Thus, it is implied that $J(\boldsymbol{r}_o, t)$ needs to be continuous and consequently, $\boldsymbol{v}$ needs to be continuously differentiable (at least piecewise) in the fundamental region. The latter is rather a restriction

on the constitutive model and macro–micro linking assumption that is used to compute $\boldsymbol{v}$. The differentiability of $\boldsymbol{v}$ also ensures the invertibility of the map from $\boldsymbol{r}_o$ to $\boldsymbol{r}_t$. The computation procedure of the reorientation velocity in the cubochoric space is explained in section 3.2 using a numerical technique. The identification of the reorientation velocity also leads to the computation of the Jacobian of the ODF evolution expression in terms of the cubochoric coordinates. Thus, the texture evolution is studied in the cubochoric space using the finite element approach.

To compute the ODF evolution, the fundamental region is meshed using tetrahedral elements, and the evolution equation is solved using a stabilized finite element method [13]. The reorientation velocity is evaluated through crystal constitutive relations. In the application shown in the ensuing sections, texturing in fcc materials with twelve $\{111\}\langle 110\rangle$ slip systems is modeled using a rate-dependent viscoplastic Taylor model with material parameters taken from [23].

2.3. Crystal constitutive equations

The micro-macro linking approach in this work is similar to the crystal constitutive relations presented by Kumar and Dawson [13], and explained in more detail in [24, 25]. The classical single crystal plasticity theory, presented previously by Taylor [1], Mandel [26], Rice [27], Mandel [28], Hill [29], Teodosiu and Sidoroff [30], Asaro [31], Asaro and Needleman [2], Bronkhorst *et al* [32], and Cuitino and Ortiz [33], is employed. According to this model the deformations are assumed to be largely monotonic and therefore the elastic effects are ignored. This model is based on the notion that plastic flow takes place through slip on prescribed slip systems. A rate-independent version of the single crystal plasticity model developed by Anand and Kothari [34] is used to model the single crystal constitutive response and is summarized below.

For a material with $\alpha = 1, \ldots, N$ slip systems defined by ortho-normal vector pairs ($\boldsymbol{m}^\alpha$, $\boldsymbol{n}^\alpha$) denoting the slip direction and slip plane normal respectively, the constitutive equations relate the following basic fields: the Cauchy stress, $\boldsymbol{T}$, the slip resistances, $s^\alpha > 0$, and the deformation gradient $\boldsymbol{F}$ which can be decomposed into elastic and plastic parts as $\boldsymbol{F} = \boldsymbol{F}^e\boldsymbol{F}^p$ with $\det(\boldsymbol{F}^p) = 1$. In the constitutive equations, which characterize small elastic strains, the Green elastic strain measure $\bar{\boldsymbol{E}} = \frac{1}{2}(\boldsymbol{F}^{eT}\boldsymbol{F}^e - \boldsymbol{I})$ is defined on the relaxed configuration (plastically deformed, unstressed configuration). The conjugate stress measure is then defined as $\bar{\boldsymbol{T}} = \det(\boldsymbol{F}^e)(\boldsymbol{F}^e)^{-1}\boldsymbol{T}(\boldsymbol{F}^e)^{-T}$ where $\boldsymbol{T}$ is the Cauchy stress for the crystal in the sample reference frame.

The constitutive relation, for stress, is given by $\bar{\boldsymbol{T}} = \boldsymbol{\mathcal{L}}^e[\bar{\boldsymbol{E}}^e]$ where $\boldsymbol{\mathcal{L}}^e$ is the fourth-order anisotropic elasticity tensor. In this constitutive model, it is assumed that deformation takes place in a single crystal through dislocation glide and the evolution of the plastic flow is given by equation (8):

$$\boldsymbol{L}^p = \dot{\boldsymbol{F}}^p(\boldsymbol{F}^p)^{-1} = \sum_\alpha \dot{\gamma}^\alpha \boldsymbol{S}_0^\alpha \operatorname{sign}(\tau^\alpha), \tag{8}$$

where $\boldsymbol{S}_0^\alpha = m^\alpha \otimes n^\alpha$ is the Schmid tensor, $\dot{\gamma}^\alpha$ is the plastic shearing rate on slip system α. The resolved stress on the αth slip system is given by $\boldsymbol{\tau}^\alpha = \bar{\boldsymbol{T}}\dot{\boldsymbol{S}}_0^\alpha$. The resolved shear stress, $\boldsymbol{\tau}^\alpha$, attains a critical value s^α on the systems where slip occurs ($\dot{\gamma}^\alpha > 0$). Furthermore, the resolved shear stress does not exceed s^α on the inactive systems with $\dot{\gamma}^\alpha = 0$. The hardening law for the slip resistance, s^α, is taken as in equation (9):

$$\dot{s}^{\alpha}(t) = \sum_{\beta} h^{\alpha\beta}\dot{\gamma}^{\beta}, \quad \text{with} \quad s^{\alpha}(0) = s_0^{\alpha}. \tag{9}$$

A constitutive time-integration procedure for the rate-independent crystal plasticity model is detailed in Anand and Kothari [34]. The constitutive problem is solved at every integration point in a reference fundamental region attached to a macroscopic material point. For computing texture evolution, the reorientation velocity is calculated using equation (3).

3. Texture evolution over cubochoric space

3.1. Coordinate transformation

The main goal of this paper is to represent the texture evolution in cubochoric space. There is no simple analytical coordinate transformation between Rodrigues and cubochoric spaces. However, it is possible to convert the Rodrigues parameters to an intermediate coordinate system, homochoric coordinates, and then convert the homochoric coordinates to the cubochoric space. The homochoric representation is an equal-volume parameterization of rotation space so that a uniform sampling in homochoric space provides a uniform sampling of the rotation space. The cubochoric representation provides a simple mapping on a 3D cubic grid to sample uniformly in the rotation space. The transformation algorithm from Rodrigues space to cubochoric space will be divided into two parts as the transformation from Rodrigues to homochoric, and from homochoric to cubochoric, and the algorithms are detailed in the following sections.

3.1.1. Transformation of Rodrigues vector to homochoric vector. Starting from a Rodrigues vector with length r, the homochoric vector, $\boldsymbol{h}$, can be obtained using:

$$\boldsymbol{h} = \bar{\boldsymbol{n}} f^{\frac{1}{3}}, \tag{10}$$

where $f = 3(\phi - \sin\phi)/4$ and $\phi = 2\arctan(r)$. There are two special cases: $r = 0 \rightarrow f = 0$, and when r goes to infinity then f goes to $3\pi/4$.

3.1.2. Transformation of homochoric vector to cubochoric vector. Given the homochoric vector, $\boldsymbol{h}$, the cubochoric vector, $\boldsymbol{c}$, can be calculated using the steps listed in figure 1 [35]. Here, the homochoric vector, $\boldsymbol{h}$, can be calculated using the formulation given in section 3.1.1. The cubochoric space is consisted of three pyramidal regions. As explained in figure 1, the conversion of the homochoric vector to the cubochoric vector depends on which of these pyramidal sections the homochoric vector transforms into.

3.2. Modeling texture evolution

Texture evolution is driven by the reorientation velocity given in equation (3). Therefore, the expressions for the reorientation velocity and its gradient should be derived in cubochoric space to represent the texture evolution. The derivation starts with differentiating equation (1):

$$\boldsymbol{v} = f\dot{\boldsymbol{n}} + f'\dot{\phi}\boldsymbol{n}; \tag{11}$$

The relations for the rates of invariants were provided in [36]:

$$\dot{\phi} = \boldsymbol{n} \cdot \boldsymbol{\omega}; \tag{12}$$

$$\dot{\boldsymbol{n}} = \frac{\sin\phi}{2(1 - \cos\phi)}\boldsymbol{n} \times \boldsymbol{\omega} \times \boldsymbol{n} + \frac{1}{2}\boldsymbol{\omega} \times \boldsymbol{n}. \tag{13}$$

1. Make sure that $|\mathbf{h}| \leq (3\pi/4)^{1/3}$; if not, return zero-vector and error status 1.
2. If this is the identity rotation, then return the zero-vector and error status 0.
3. Determine which pyramidal section $\mathbf{h}$ is part of, and rearrange the components h_i accordingly: pyramids $1, 2 \rightarrow$ no change; $3, 4 \rightarrow \mathbf{h} = (h_2, h_3, h_1)$; $5, 6 \rightarrow \mathbf{h} = (h_3, h_1, h_2)$.
4. Using the rearranged $\mathbf{h}$, put $q = (2|\mathbf{h}|/(|\mathbf{h}| + |h_3|))^{1/2}$; then compute

$$\mathbf{h}' = \left(qh_1, qh_2, \text{sign}(h_3)|\mathbf{h}|/\sqrt{6/\pi}\right)$$

5. Set $qxy = h_1'^2 + h_2'^2$; if $h_1' \neq 0 \rightarrow sx = \text{sign}(h_1')$, else $sx = 1$; if $h_2' \neq 0 \rightarrow sy = \text{sign}(h_2')$, else $sy = 1$;
6. if $|h_2'| \leq |h_1'|$ then compute

$$\begin{aligned} q2xy &= qxy + h_1'^2; \\ sq2xy &= \sqrt{q2xy}; \\ q &= \frac{\pi^{5/6}4^{1/3}}{2\sqrt{2}\,(3\pi)^{1/3}6^{1/6}}\sqrt{\frac{q2xy\,qxy}{(q2xy - |h_1'|sq2xy)}}; \\ ac &= \arccos((h_2'^2 + |h_1'|sq2xy)/\sqrt{2}/qxy); \\ T1inv &= q\,sx; \\ T2inv &= 12q\,sy\,ac/\pi. \end{aligned}$$

else $(|h_1'| \leq |h_2'|)$

$$\begin{aligned} qx2y &= qxy + h_2'^2; \\ sqx2y &= \sqrt{qx2y}; \\ q &= \frac{\pi^{5/6}4^{1/3}}{2\sqrt{2}\,(3\pi)^{1/3}6^{1/6}}\sqrt{\frac{qx2y\,qxy}{(qx2y - |h_2'|sqx2y)}}; \\ ac &= \arccos((h_1'^2 + |h_2'|sqx2y)/\sqrt{2}/qxy); \\ T1inv &= 12q\,sx\,ac/\pi; \\ T2inv &= q\,sy. \end{aligned}$$

Then set $\mathbf{h}'' = (6/\pi)^{1/6}(T1inv, T2inv, h_3')$

7. Finally, revert the components back to the original order (undoing the pyramid case): $1, 2 \rightarrow \mathbf{c} = \mathbf{h}''$; $3, 4 \rightarrow \mathbf{c} = (h_3'', h_1'', h_2'')$; and $5, 6 \rightarrow \mathbf{c} = (h_2'', h_3'', h_1'')$. Return $\mathbf{c}$ and error status 0.

Special cases: None (already dealt with in steps 1 and 2)

Figure 1. The computational algorithm for transformation of homochoric vector to cubochoric vector. Reproduced with permission from [35].

Using the previously given expression for the spin vector $\boldsymbol{\omega}$, the reorientation velocity $\boldsymbol{v}$ can be written in the form:

$$\boldsymbol{v} = \frac{1}{2}\boldsymbol{B}\boldsymbol{\omega}, \tag{14}$$

where:

$$\boldsymbol{B} = \frac{f\sin\phi}{1 - \cos\phi}\boldsymbol{I} + \left(\frac{2f'}{f} - \frac{\sin\phi}{1 - \cos\phi}\right)\boldsymbol{n} \otimes \boldsymbol{n} + \boldsymbol{I} \times \boldsymbol{n}. \tag{15}$$

Equation (15) shows that the reorientation velocity, $\boldsymbol{v}$ is composed of three components along $\boldsymbol{\omega}$, $\boldsymbol{n}$ and $\boldsymbol{\omega} \times \boldsymbol{n}$ respectively, and therefore the discretization of $\boldsymbol{\omega}$ in the constitutive model is advantageous. Using the same procedure the orientation update on the cubochoric space can be performed with the transformation of the Rodrigues vector to the cubochoric vector

$$\boldsymbol{r}_c = \text{cubochoric transformation } (\boldsymbol{r}); \tag{16}$$

$$\boldsymbol{B}_c = \boldsymbol{B}(\boldsymbol{r}_c), \tag{17}$$

where the cubochoric transformation function in equation (16) symbolizes the numerical operations required to transform the Rodrigues parameters to the cubochoric vector. Therefore $\boldsymbol{r}_c$ and $\boldsymbol{r}$ denote the cubochoric and Rodrigues vectors; $\boldsymbol{B}_c$ is the $\boldsymbol{B}$ matrix, defined in equation (15), in cubochoric coordinates; $\boldsymbol{B}_c$ can be written in terms of the Rodrigues parameters by eliminating the dependency on rotation angle, ϕ

$$\boldsymbol{B}_c = f\frac{1}{\rho}\boldsymbol{I} + \left(\frac{2f'}{f} - \frac{1}{\rho}\right)\frac{1}{1/\rho^2}\boldsymbol{r}\boldsymbol{r}^T - \frac{\boldsymbol{r}^{\times}}{\rho}, \tag{18}$$

where $\rho = (\boldsymbol{r}^T\boldsymbol{r})^{\frac{1}{2}}$ is the magnitude of the Rodrigues vector, and $\boldsymbol{r}^{\times}$, is the cross operator [37] of two Rodrigues vectors. Since the cubochoric transformation is not directly neo-Eulerian, the f can only be computed numerically. The computation of the derivative term, f', is also numerical, and its details are given below:

$$f' = \frac{\partial f}{\partial \phi} = \frac{\partial f}{\partial \boldsymbol{r}} \cdot \frac{\partial \boldsymbol{r}}{\partial \phi}; \tag{19}$$

using a central differencing scheme this derivative can be written as:

$$\frac{\partial f}{\partial \phi} = \frac{\partial f}{\partial \boldsymbol{r}} \cdot \frac{\partial \boldsymbol{r}}{\partial \phi} = \frac{f(\boldsymbol{r} + \Delta\boldsymbol{r}) - f(\boldsymbol{r} - \Delta\boldsymbol{r})}{2\Delta\boldsymbol{r}} \cdot \frac{\boldsymbol{r}(\phi + \Delta\phi) - \boldsymbol{r}(\phi - \Delta\phi)}{2\Delta\phi}. \tag{20}$$

Then the reorientation velocity can be computed using the following equation:

$$\boldsymbol{v}_c = \frac{\mathrm{d}\boldsymbol{r}_c}{\mathrm{d}t} = \frac{1}{2}\boldsymbol{B}_c\boldsymbol{\omega}. \tag{21}$$

In equation (21), the reorientation velocity, $\boldsymbol{v}_c$, is written as a time derivative of the orientation in cubochoric coordinates. The new orientation in cubochoric space is then found as:

$$\boldsymbol{r}_c^{i+1} = \boldsymbol{r}_c^i + \left(\frac{\partial \boldsymbol{r}_c^i}{\partial t}\mathrm{d}t\right), \tag{22}$$

where $\boldsymbol{r}_c^i$ and $\boldsymbol{r}_c^{i+1}$ are the cubochoric vectors at time iterations i and $i + 1$ respectively.

4. Applications

In this work, the texture evolution in three different deformation processes (tension, plane strain compression and shear) was analyzed in cubochoric space for a fcc material. The strain rate was taken as 1×10^{-3}. The finite element discretization is performed for a mesh including 145 independent nodal points. The fundamental region meshes for an fcc material in Rodrigues and cubochoric spaces are illustrated in figure 2.

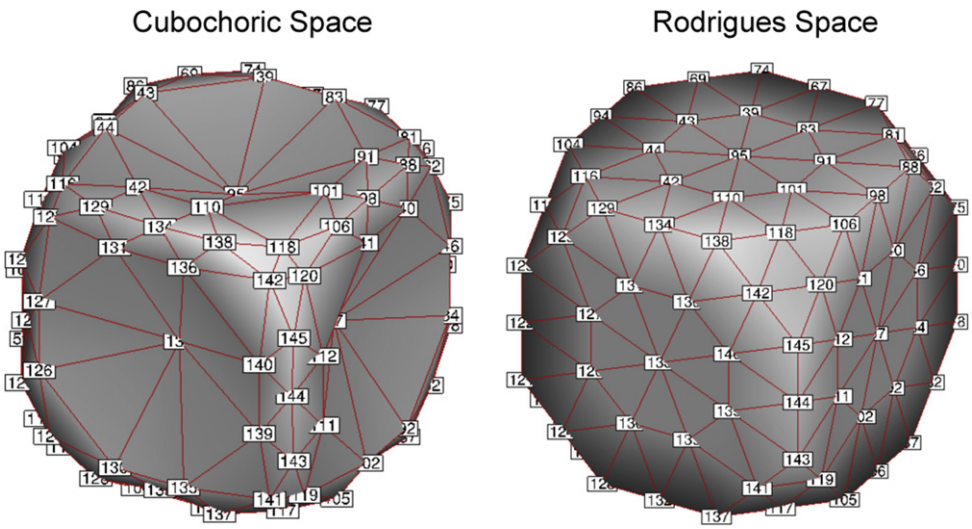

Figure 2. Fundamental regions of Rodrigues and cubochoric spaces.

4.1. Tension

The first application is a tension acting along the x-direction, and the corresponding velocity gradient, L, is given by [7]:

$$L = \begin{bmatrix} 1 & 0 & 0 \\ 0 & -0.5 & 0 \\ 0 & 0 & -0.5 \end{bmatrix}. \tag{23}$$

The simulation was performed for 1000 time steps discretizing the ODF in both Rodrigues and cubochoric spaces. The final textures obtained using both discretizations are compared to each other in figure 3. The textures are also compared by using ⟨111⟩, ⟨100⟩, ⟨110⟩ pole figures as shown in figure 4.

Analyzing the similarities in texture evolution in both spaces can be difficult since the nodal coordinates of the Rodrigues space are different in cubochoric space. This causes problems since any 2D section of these 3D spaces would not be representative for the same feature. However, by looking at the 3D comparison it can be concluded that the texture evolution for fcc copper material shows very similar features in Rodrigues and cubochoric spaces since the ODF intensities and the texture layout match in nodal points. The ODF map in the Rodrigues domain also agrees well with the illustrations in [13, 38].

4.2. Plane strain compression

The second application simulates a plane strain compression test, and the corresponding velocity gradient, L, is provided in equation (24)

$$L = \begin{bmatrix} 0 & 0 & 0 \\ 0 & 1 & 0 \\ 0 & 0 & -1 \end{bmatrix}. \tag{24}$$

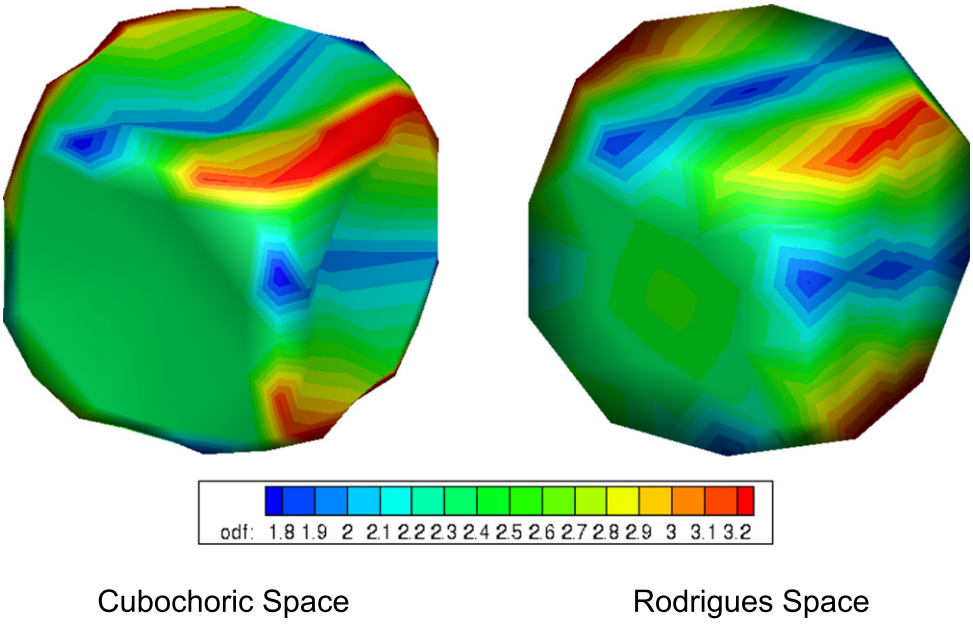

Figure 3. Texture evolution during tension in Rodrigues and cubochoric spaces.

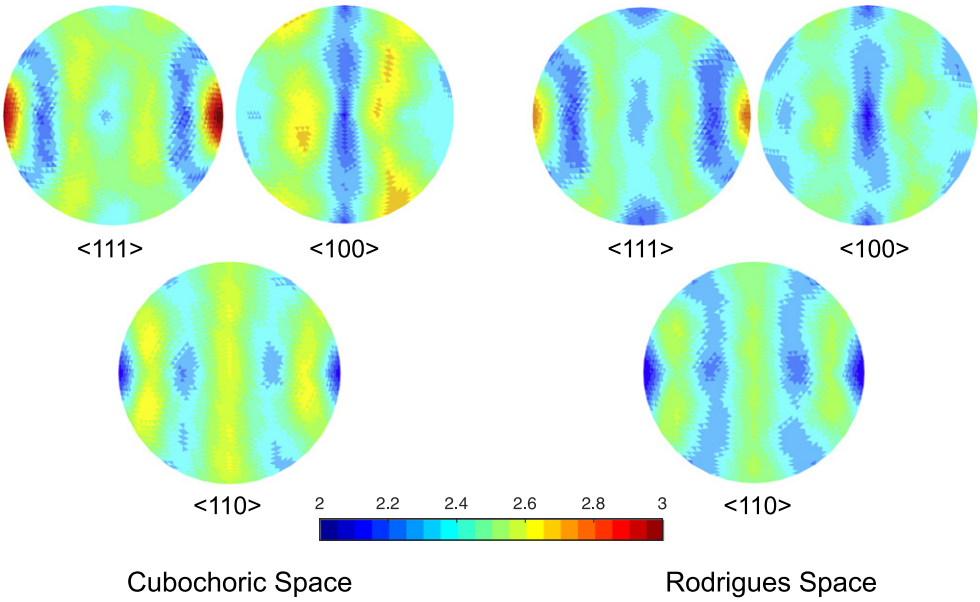

Figure 4. Comparison of pole figures in Rodrigues and cubochoric spaces for the tension test.

The simulation was again performed for 1000 time steps discretizing the ODF in both Rodrigues and cubochoric spaces. The final textures obtained using both discretizations are compared to each other in figure 5, and the pole figures are also compared in figure 6.

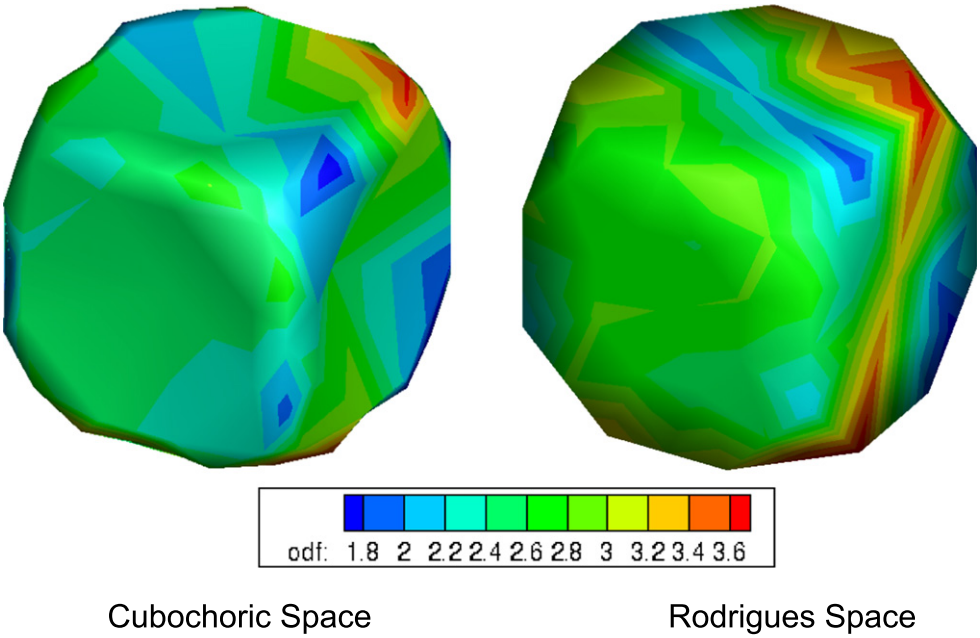

Figure 5. Texture evolution during plane strain compression in Rodrigues and cubochoric spaces.

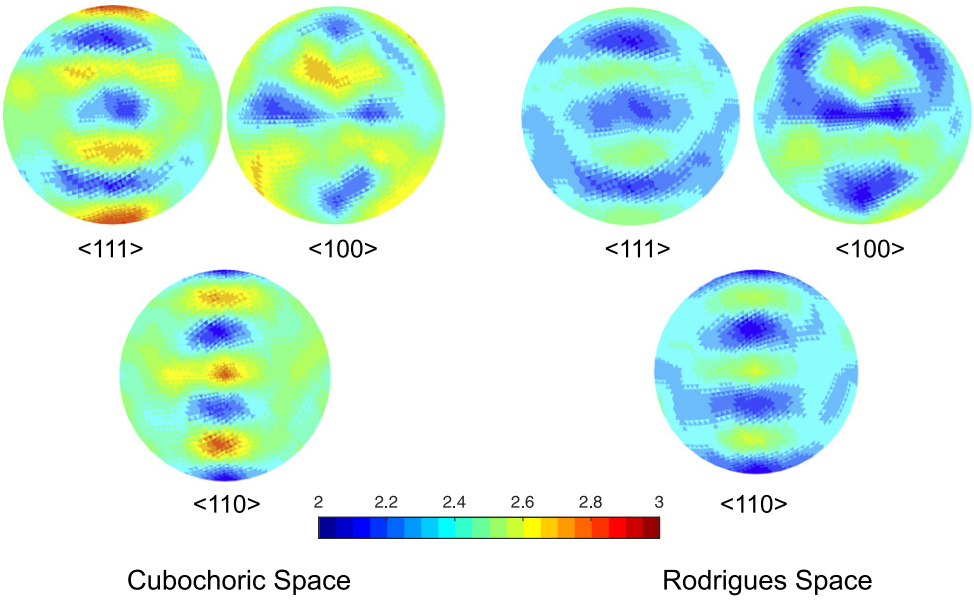

Figure 6. Comparison of pole figures in Rodrigues and cubochoric spaces for the plane strain compression test.

Making a direct comparison between sections through the Rodrigues and cubochoric spaces is again very hard in this case, but similar patterns can be observed in the 3D space representations of texture evolution depicted in figure 5 for the plane strain compression test.

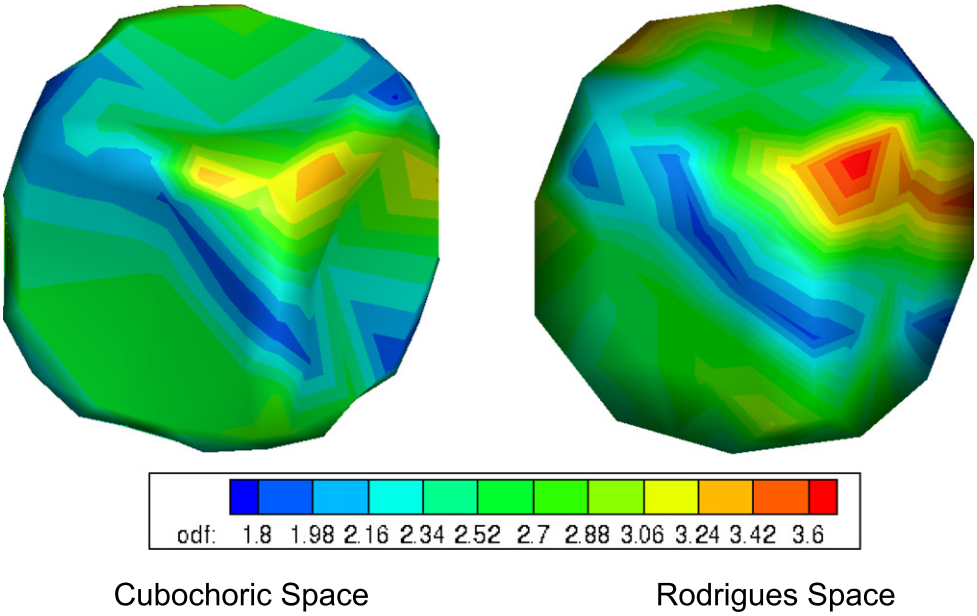

Figure 7. Texture evolution during *xy*-shear in Rodrigues and cubochoric spaces.

4.3. Shear

The last application is the simulation for *xy*-shear. The corresponding velocity gradient, L, is given in equation (25)

$$L = \begin{bmatrix} 0 & -1 & 0 \\ 1 & 0 & 0 \\ 0 & 0 & 0 \end{bmatrix}. \tag{25}$$

The simulation was performed for 1000 time steps discretizing the ODF in both Rodrigues and cubochoric spaces. The final textures obtained using both discretizations are compared to each other in figure 7. In figure 8, the pole figures are compared.

In figure 7 similar patterns are observed in the 3D texture evolution representations in Rodrigues and cubochoric spaces.

The results illustrated in figures 3–8 indicate that the texture evolution over both orientation spaces shows similar features. This is also shown here quantitatively by defining an error metric between the ODF vectors of the Rodrigues domain and the cubochoric domain: $e = \sum_{i=1}^{n}(A_r(i) - A_c(i))^2$, where A_r is the ODFs in the Rodrigues space, A_c is the ODFs in the cubochoric space, and n is the total number of the ODFs. The numerical values of the ODF differences for each case are given in table 1. As shown in table 1, the differences between the ODFs are very small as can be interpreted by the direct comparison with the mean values of the ODFs in both spaces. Thus, the texture evolution over the Rodrigues and cubochoric space is found to be quantitatively similar as well. In table 1, μ_{A_r} and μ_{A_c} show the mean ODF values over the Rodrigues and cubochoric domains.

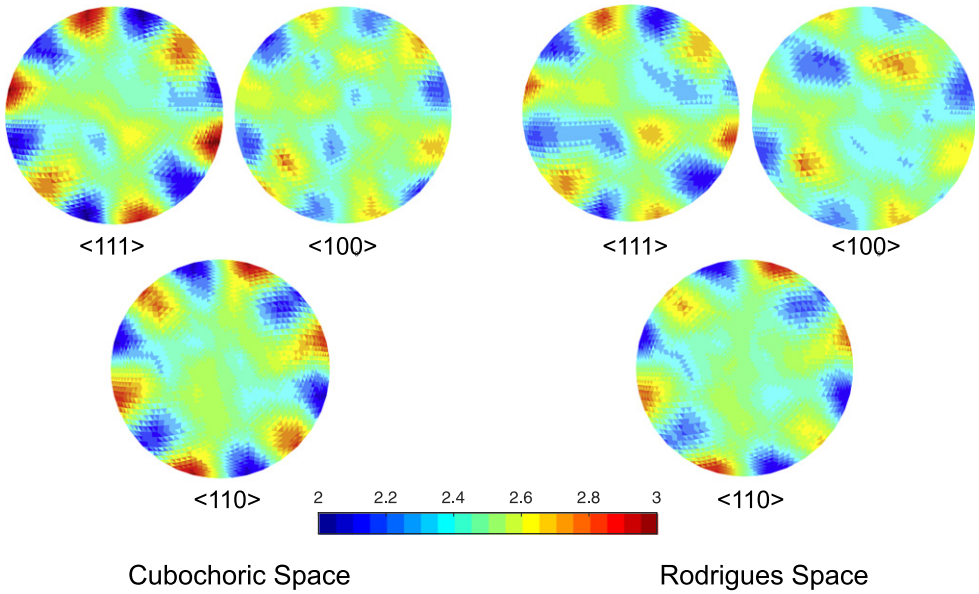

Figure 8. Comparison of pole figures in Rodrigues and cubochoric spaces for the shear test.

Table 1. Comparison of the ODFs over the Rodrigues and cubochoric spaces.

Case	Rodrigues domain	Cubochoric domain	Error metric
Tension	$\mu_{A_r} = 2.4091$	$\mu_{A_c} = 2.4766$	$e = 0.0073$
Plane strain compression	$\mu_{A_r} = 2.4129$	$\mu_{A_c} = 2.4608$	$e = 0.0237$
xy-shear	$\mu_{A_r} = 2.4626$	$\mu_{A_c} = 2.4755$	$e = 0.0134$

5. Conclusions

The texture evolution of an fcc microstructure in different orientation spaces is discussed. The microstructure is quantified with the one-point probability descriptor, ODF, and the texture evolution is represented with the evolution of the ODF, which is governed by a conservation equation and a crystal constitutive model. The ODF is first discretized with a finite element scheme in Rodrigues space. Next, the finite element mesh in Rodrigues space, including 145 nodal points, is transformed into a new domain, cubochoric space. The cubochoric space is preferred in this work since it has recently become an alternative 3D uniform sampling space for dictionary based indexing of crystalline diffraction patterns. It represents an equal-volume transformation, and it is very advantageous to work with in microstructures since it accounts for crystallographic symmetries. The cubochoric orientation space leads to a homogenous nodal point representation of the microstructures because of the cubical shape. This makes the determination of the fundamental regions easier compared to the other orientation spaces. The finite element nodal points can be identified with uniform sampling approaches in the cubochoric space. However, the locations of the finite element nodes cannot be found with a straightforward approach when using other techniques. Thus, the quantification of the experimental texture is more convenient with the cubochoric space parameters. Our goal in this work is to derive a finite

element approach in the cubochoric space that produces equivalent results with the Rodrigues representation. With this purpose, the constitutive relations are also updated accordingly for the computation of the reorientation velocity in the cubochoric space. The Lagrangian representation of the ODF evolution equation is used. The computation of the reorientation velocity in the cubochoric space using numerical techniques enabled the identification of the deformation gradient of the cubochoric space as well. Since the Lagrangian ODF representation is fundamentally driven by the Jacobian value, which is directly related to the deformation gradient, the texture evolution is solved in the cubochoric space with the finite element approach. Next, the texture evolution during tension, plane strain compression and shear deformation processes is analyzed in cubochoric space; it is found that the ODF distribution shows very similar patterns in 3D cubochoric space representation with the 3D representation in Rodrigues space. Transformation from Rodrigues space to cubochoric space becomes numerically complicated as the number of independent nodal points increases. Future work will focus on overcoming these complexities and on the transformation of a finer mesh from Rodrigues space to cubochoric space. The texture evolution of materials having different crystallographic structures, such as HCP materials, can also be analyzed in cubochoric space as a future work. Another future area may be the application of the same finite element approach to cubochoric maps with different crystal symmetries.

Acknowledgments

M De Graef would like to acknowledge financial support from an ONR Vannevar Bush Faculty Fellowship N00014-16-1-2821.

ORCID iDs

Pınar Acar https://orcid.org/0000-0002-5911-0410
Veera Sundararaghavan https://orcid.org/0000-0002-1213-7958

References

[1] Taylor G 1938 Plastic strain in metals *J. Inst. Met.* **62** 307–24
[2] Asaro R J and Needleman A 1985 Texture development and strain hardening in rate dependent polycrystals *Acta Metall.* **33** 923–53
[3] Canova G R, Kocks U F and Jonas J J 1984 Theory of torsion texture development *Acta Metall.* **32** 211–26
[4] Molinari A, Canova G R and Ahzi S 1987 A self consistent approach of the large deformation polycrystal viscoplasticity *Acta Metall.* **35** 2983–94
[5] Tiem S, Berveiller M and Canova G R 1986 Grain shape effects on the slip system activity and on the lattice rotations *Acta Metall.* **34** 2139–49
[6] Acar P and Sundararaghavan V 2016 Linear solution scheme for microstructure design with process constraints *AIAA J.* **54** 4022–31
[7] Sundararaghavan V and Zabaras N 2005 On the synergy between texture classification and deformation process sequence selection for the control of texture-dependent properties *Acta Mater.* **53** 1015–27
[8] Bunge H J 1982 *Texture Analysis in Materials Science* (London: Butterworths)
[9] Kocks U F, Tome C N and Wenk H R 2000 *Texture and Anisotropy* (Cambridge: Cambridge University Press)
[10] Heinz A and Neumann P 1991 Representation of orientation and disorientation data for cubic, hexagonal, tetragonal and orthorhombic crystals *Acta Crystallogr.* **A47** 780–9
[11] Adams B L, Henrie A, Henrie B, Lyon M, Kalidindi S R and Garmestani H 2001 Microstructure-sensitive design of a compliant beam *J. Mech. Phys. Solids* **49** 1639–63

[12] Kalidindi S R, Houskamp J, Lyons M and Adams B L 2004 Microstructure sensitive design of an orthotropic plate subjected to tensile load *Int. J. Plast.* **20** 1561–75
[13] Kumar A and Dawson P R 2000 Computational modeling of F.C.C. deformation textures over Rodrigues' space *Acta Mater.* **48** 2719–36
[14] Kumar A and Dawson P R 2000 Modeling crystallographic texture evolution with finite elements over neo-Eulerian orientation spaces *Comput. Methods Appl. Mech. Eng.* **153** 259–302
[15] Barton N R, Bernier J V, Lebensohn R A and Boyce D E 2015 The use of discrete harmonics in direct multi-scale embedding of polycrystal plasticity *Comput. Methods Appl. Mech. Eng.* **283** 224–42
[16] Acar P and Sundararaghavan V 2016 Utilization of a linear solver for multiscale design and optimization of microstructures *AIAA J.* **54** 1751–9
[17] Chen Y H, Park S U, Wei D, Newstadt G, Jackson M A, Simmons J P, De Graef M and Hero A O 2015 A dictionary approach to electron backscatter diffraction indexing *Microsc. Microanal.* **21** 739–52
[18] Singh S and De Graef M 2016 Orientation sampling for dictionary-based diffraction pattern indexing methods *Modelling Simul. Mater. Sci. Eng.* **24** 085013
[19] Yershova A and LaValle S M 2004 Deterministic sampling methods for spheres and SO(3) *IEEE Proc. ICRA 04* vol 4 pp 3974–80
[20] Yershova A, Jain S, LaValle S M and Mitchell J C 2010 Generating uniform incremental grids on SO(3) using the Hopf fibration *Int. J. Robot. Res.* **29** 801–12
[21] Gorski K M, Hivon E, Banday A J, Wandelt B D, Hansen F K, Rei-Necke M and Bartelmann M 2005 HEALPix: a framework for high-resolution discretization and fast analysis of data distributed on the sphere *Astrophys. J.* **622** 759–71
[22] Roşca D, Morawiec A and De Graef M 2014 A new method of constructing a grid in the space of 3D rotations and its applications to texture analysis *Modelling Simul. Mater. Sci. Eng.* **22** 075013
[23] Acharjee S and Zabaras N 2003 A proper orthogonal decomposition approach to microstructure model reduction in Rodrigues space with applications to the control of material properties *Acta Mater.* **51** 5627–46
[24] Sundararaghavan V and Zabaras N 2006 Design of microstructure-sensitive properties in elasto-viscoplastic polycrystals using multi-scale homogenization *Int. J. Plast.* **22** 1799–824
[25] Sundararaghavan V and Zabaras N 2008 A multi-length scale sensitivity analysis for the control of texture-dependent properties in deformation processing *Int. J. Plast.* **24** 1581–605
[26] Mandel J 1965 Generalization de la theorie de la plasticite de W T Koiter *Int. J. Solids Struct.* **1** 273–95
[27] Rice J R 1971 Inelastic constitutive relations for solids: an internal variable theory and its application to metal plasticity *J. Mech. Phys. Solids* **19** 433–55
[28] Mandel J 1972 Plasticite Classique et Viscoplasticite *CISM Courses and Lectures* vol 97 (Berlin: Springer)
[29] Hill R 1965 Continuum micro-mechanics of elastoplastic polycrystals *J. Mech. Phys. Solids* **13** 89–101
[30] Teodosiu C and Sidoroff F 1976 A theory of finite elastoviscoplasticity of single crystals *Int. J. Eng. Sci.* **14** 165–76
[31] Asaro R J 1983 Micromechanics of crystals and polycrystals *Adv. Appl. Mech.* **23** 1–115
[32] Bronkhorst C A, Kalidindi S R and Anand L 1992 Polycrystalline plasticity and the evolution of crystallographic texture in FCC metals *Phil. Trans. R. Soc.* A **341** 443–77
[33] Cuitino A M and Ortiz M 1992 Computational modeling of single crystals *Modelling Simul. Mater. Sci. Eng.* **1** 225–63
[34] Anand L and Kothari M 1996 A computational procedure for rate-independent crystal plasticity *J. Mech. Phys. Solids* **44** 525–58
[35] DeGraef M 2014 A Fortran-90 implementation of rotation representations *Multidisciplinary University Research Initiative document*
[36] Angeles J 1988 *Rotational Kinematics* (New York: Springer)
[37] D'Eleutario G M T and Heppler G R 2011 *Newton's Second Law And All That* (Cambridge: Cambridge University Press) pp 523–6
[38] Kumar A and Dawson P R 2009 Dynamics of texture evolution in face-centered cubic polycrystals *J. Mech. Phys. Solids* **57** 422–45